Computer Simulation of Morphologies and Optical Properties of Filled Diblock Copolymers

Gavin A. Buxton, Jae Youn Lee, and Anna C. Balazs*

Department of Chemical and Petroleum Engineering, University of Pittsburgh, Pittsburgh, Pennsylvania 15261

Received March 14, 2003; Revised Manuscript Received October 2, 2003

ABSTRACT: We integrate two computational techniques in order to determine the optical properties of self-assembled mixtures of diblock copolymers and nanoparticles. To determine the morphology of the system, we first use an approach that combines a self-consistent-field theory (SCFT) for the diblocks with a density functional theory (DFT) for the particles. Using this SCF/DFT model, we focus on the lamellar phase of AB diblocks and calculate volume fraction profiles for systems containing selective or nonselective nanoparticles. We use the volume fraction profiles from the SCF/DFT and assign typical dielectric constants for the different polymer domains and the particles to characterize the dielectric properties of the composite. A finite difference time domain (FDTD) technique is then used to simulate the propagation of light through this heterogeneous material. The results of this study allow us to determine how the polymer−particle interactions affect the spatial distribution of fillers within the polymer matrix and how this distribution in turn affects the optical properties of the nanocomposite. The findings can provide guidelines for facilitating the design of photonic band gap materials.

1. Introduction

In photonic crystals, the dielectric constant of the material is a spatially periodic function. In such systems, forbidden frequency bands can exist for incident electromagnetic waves. These photonic band gaps are caused by the interference of waves as they are reflected and scattered by regularly spaced regions of varying dielectric properties. Block copolymers have the potential to form promising photonic crystals due to the fact they self-assemble into spatially periodic materials.[1] Because of limitations on the molecular weight of the polymer species (and therefore the domain sizes) and the dielectric contrast between different blocks, the range of forbidden frequencies and the size of the photonic band gaps are severely restricted. Thomas et al.[2,3] have successfully swollen domain sizes through the addition of homopolymers in order to shift photonic band gaps from the ultraviolet to the visible region of the spectrum. It was also shown that the width of the band gap could be increased through the selective sequestering of inorganic nanocrystals within one of the phases of the microphase-separated diblock copolymers.[3−5]

Recent computational investigations into the self-assembly of nanoparticles and diblock copolymers have provided significant insight into the possible morphologies of such structures. In particular, Balazs et al. have developed a "SCF/DFT" approach that combines self-consistent-field theory (SCFT) for diblocks and density functional theory (DFT) for particles to examine how the characteristics of the polymers and particles affect the structure of the resultant hybrid material.[6−11] Experimental studies[12] have recently confirmed the SCF/DFT predictions on the entropically driven size segregation of binary particle mixtures within a diblock melt.[7,9] Experiments[13] have also validated the prediction that added nanoparticles can promote transitions between the different structures of the diblock copolymers.[8] In addition, recent Monte Carlo simulations[14] support the finding[8] that neutral nanoparticles will localize at the A/B interface of the AB diblocks. As the particle size is decreased (at a fixed volume fraction),[8] the SCF/DFT results indicate that while some portion of the neutral particles remain at the A/B interface, the smaller particles become more delocalized and extend into the A and B domains; the SCF/DFT density profiles for this system show qualitative agreement with density profiles for neutral solvents in diblock copolymers.[15]

In this paper we extend this work by combining the SCF/DFT morphological studies with a computational model for the propagation of light. Using this integrated approach, we determine the optical properties of the self-assembled composite.

To model the propagation of light through this diblock/nanoparticle composite, we use the finite difference time domain (FDTD) method, which is a flexible, numerical means of analyzing interactions between waves and complex materials containing dielectric or metallic objects.[16] The technique involves approximating the integration of Maxwell's equations in real space by the use of finite differences. Specifically, the FDTD is a "time marching" algorithm used to solve the wave equation at each point on a grid.[17] The field is set to zero at the initial time step, and at the next time step, a source is turned on to generate an optical signal. From this initial condition, the wave fields at all points on the grid at any later time can be calculated through a simple, iterative scheme. The FDTD technique is highly useful for examining the behavior of heterogeneous materials[18] since one can readily compute the propagation of light in materials that include particles of arbitrary shape or interparticle distance.[17]

In the present study, we assume that the diblock copolymer structures are perfectly aligned, periodic lamellae. Such regular structures can more readily be attained in thin films.[4] We find that even for this simple 1D photonic band gap material, a rich variety of phenomena can be observed.

* Corresponding author. E-mail: balazs1@engr.pitt.edu.

10.1021/ma034322+ CCC: $25.00
Published on Web 11/13/2003

2. Methodology

2.1. SCF/DFT. To determine the structure of the system, we use our hybrid SCF/DFT model for incompressible mixtures of diblock copolymers and spherical nanoparticles. Below, we briefly summarize the model and refer the reader to ref 11 for a more detailed description of this technique. The SCF/DFT constitutes a powerful method for determining the phase behavior of the system because we are not constrained to make a priori assumptions about the structure of the phase or the distribution of particles. In SCF theory, pairwise interactions between differing segments are replaced by the interaction of each segment with the average field created by the other segments. Here, we let $w_A(\mathbf{r})$ denote the mean field felt by the A segments at $\mathbf{r}$, $w_B(\mathbf{r})$ denote the field for B segments, and $w_p(\mathbf{r})$ represent the field for particles. Using this approach, the free energy for our system is given by $F_T = F_e + F_d + F_p$. The first term, F_e, details the enthalpic interactions:

$$F_e = \frac{1}{V}\int \chi_{AB}N\varphi_A(\mathbf{r})\,\varphi_B(\mathbf{r}) + \chi_{BP}N\varphi_B(\mathbf{r})\,\varphi_P(\mathbf{r}) + \chi_{AP}N\varphi_A(\mathbf{r})\,\varphi_P(\mathbf{r})\,d\mathbf{r} \quad (1)$$

where V is the volume of the system, N is the degree of polymerization of the diblock chain, and $\varphi_A(\mathbf{r})$, $\varphi_B(\mathbf{r})$, and $\varphi_P(\mathbf{r})$ are the local volume fractions of A segments, B segments, and particles, respectively. The enthalpic interaction between an A segment and a B segment is described by the dimensionless Flory−Huggins parameter, χ_{AB}. The parameters χ_{AP} and χ_{BP} describe the enthalpic interactions between the particles and the respective blocks.

The diblock entropic free energy F_d is[19]

$$F_d = (1-\phi_p)\ln\left[\frac{V(1-\phi_p)}{Q_d}\right] - \frac{1}{V}\int w_A(\mathbf{r})\,\varphi_A(\mathbf{r}) + w_B(\mathbf{r})\,\varphi_B(\mathbf{r})\,d\mathbf{r} \quad (2)$$

where Q_d is the partition function of a single diblock subject to the fields $w_A(\mathbf{r})$ and $w_B(\mathbf{r})$.

Finally, the particle entropic contributions to the free energy are given by

$$F_p = \frac{\phi_p}{\alpha}\ln\left[\frac{V\phi_p}{Q_p\alpha}\right] - \frac{1}{V}\int w_p(\mathbf{r})\,\rho_p(\mathbf{r})\,d\mathbf{r} + \frac{1}{V}\int \rho_p(\mathbf{r})\Psi_{CS}[\bar{\varphi}_p(\mathbf{r})]\,d\mathbf{r} \quad (3)$$

where Q_p is the partition function of a single particle subject to the field $w_p(\mathbf{r})$. The local particle volume fraction, $\varphi_p(\mathbf{r})$, is related to the dimensionless center of mass distribution, $\rho_p(\mathbf{r})$, by

$$\varphi_p(\mathbf{r}) = \frac{3\alpha}{4\pi R_p{}^3}\int_{|r'|<R_p}\rho_p(\mathbf{r}+\mathbf{r}')\,d\mathbf{r}' \quad (4)$$

where R_p is the radius of the particle and the parameter $\alpha = (4\pi R_p{}^3\rho_0)/(3N)$ denotes the particle-to-diblock volume ratio. Recall that the model is for an incompressible system; thus, in a mean-field manner, the incompressibility constraint prohibits significant overlap between the particles and monomers as well as significant overlap between the A and B components. However, to accurately capture the behavior of the system, we must also include a term that explicitly describes the steric interactions (the nonideal term) between the particles.[20−22] The last term of F_p describes the excess (nonideal) steric free energy of the particles through the DFT derived by Tarazona.[23,24] In particular, the Carnahan−Starling equation of state for the excess free energy of a hard-sphere fluid, Ψ_{cs}, is now evaluated with the "weighted" (locally averaged) particle volume fraction, $\bar{\varphi}_p(\mathbf{r})$.[11,23] This density functional contribution is included so that the model can describe not only homogeneous (liquid) but also inhomogeneous (crystalline) distributions of the hard spheres. We chose the Tarazona DFT because it is a simple and physical approach specifically developed to reproduce the liquid−solid transition in hard spheres.[25] Some DFTs more accurately describe the liquid equation of state but fail to predict the liquid−solid transition; other approaches are more computationally intensive. The addition of such a steric term[22] follows the example of Matsen and Barrett,[26] who used a similar approach to study rod−coil block copolymers.

We note that this approach is valid for a finite range of particles sizes. If the particle radius is beyond the root-mean-squared end-to-end distance of the chain, i.e., $R_p \gg R_o$, it may be more appropriate to view a particle as a substrate and include boundary conditions that characterize the polymer−substrate interactions. If, on the other hand, $R_p \ll R_o$, where the particle is on the same size scale as a monomer, then it may be sufficient to treat the particle as a solvent molecule. In our studies,[6−11] we have focused on cases where $0.1R_o \le R_p \le 0.3R_o$, which clearly falls in between these two extreme situations. In addition, we have focused on particle volume fractions that are less than 20% in order to ensure that mixture is not macroscopically phase-separated into a two-phase mixture.

In the SCFT, $w_A(\mathbf{r})$, $w_B(\mathbf{r})$, and $w_P(\mathbf{r})$ are determined by locating saddle points in the free energy functional F subject to the incompressibility constraint: $\varphi_A(\mathbf{r}) + \varphi_B(\mathbf{r}) + \varphi_P(\mathbf{r}) = 1$. This yields a system of equations that is solved numerically and self-consistently to give possible equilibrium solutions. To obtain these solutions, we implement the combinatorial screening technique of Drolet and Fredrickson.[27] We make an initial random guess for the fields and calculate all the volume fractions and the free energy at each step; the fields are then recalculated, and the entire process is repeated until changes in the diblock volume fractions at each step become sufficiently small. In addition, we minimize our free energy with respect to the size of the simulation box, as proposed by Bohbot-Raviv and Wang.[28]

Once we have determined the structure of the nanocomposite, we turn to the finite difference time domain (FDTD) methodology in order to model the propagation of light through this heterogeneous material.

2.2. FDTD. The FDTD methodology involves the discretization of Maxwell's curl equations of electromagnetism in three dimensions. The differential form of Maxwell's equations are[29]

$$\nabla\times\mathbf{H} = \epsilon\frac{\delta\mathbf{E}}{\delta t} + \sigma\mathbf{E} \qquad \nabla\times\mathbf{E} = -\mu\frac{\delta\mathbf{H}}{\delta t} - \sigma^*\mathbf{H} \quad (5)$$

where E is the electric field, H is the magnetic field, ϵ and μ are the permittivity and permeability, respectively, and σ and σ^* are the respective electric and magnetic conductivities. Yee[30] introduced an efficient method for implementing the FDTD method in both space and time. All the field variables are defined on a

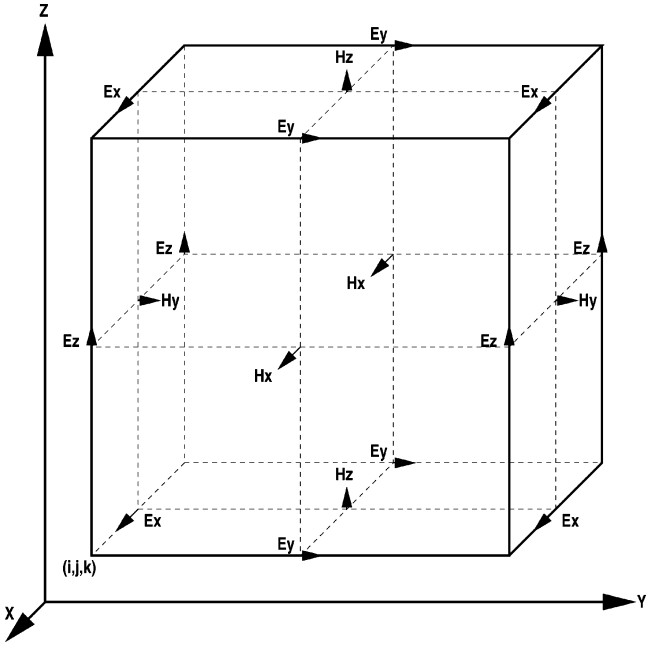

Figure 1. Positions of the field components within a Yee cell.

three-dimensional rectangular grid. In particular, the simulation region is divided into "Yee cells", where the electric fields are given at the edges of the Yee cell and the magnetic fields are given at the faces of the Yee cell, as shown in Figure 1. The FDTD method is used to calculate the electric and magnetic fields in each cell by integrating the discretized equations through a time-stepping ("leapfrog") methodology where the magnetic fields are calculated half a time step later than the electric fields. The updated electromagnetic field components are only dependent on the values at previous time steps.

In the most general form, the equations for the x components of the electric and magnetic fields are given by

$$E_x^{n+1}[i,j,k] = \frac{2\epsilon_x - \sigma_x \Delta t}{2\epsilon_x + \sigma_x \Delta t} E_x^n[i,j,k] + \frac{2\Delta t}{2\epsilon_x + \sigma_x \Delta t}\left(\frac{H_z^{n+1/2}[i,j,k] - H_z^{n+1/2}[i,j-1,k]}{\Delta y} - \frac{H_y^{n+1/2}[i,j,k] - H_y^{n+1/2}[i,j,k-1]}{\Delta z}\right) \quad (6a)$$

$$H_x^{n+1/2}[i,j,k] = \frac{2\mu_x - \sigma_x^* \Delta t}{2\mu_x + \sigma_x^* \Delta t} H_x^{n-1/2}[i,j,k] + \frac{2\Delta t}{2\mu_x + \sigma_x^* \Delta t}\left(\frac{E_y^n[i,j,k+1] - E_y^n[i,j,k]}{\Delta z} - \frac{E_z^n[i,j+1,k] - E_z^n[i,j,k]}{\Delta y}\right) \quad (6b)$$

where i, j, and k are indices representing the spatial discretization; similar expressions can be written for the y and z components. The parameters Δx, Δy, and Δz are the dimensions of the Yee cell. Time is incremented in steps of magnitude Δt and the time step given the index n. These difference equations are used for updating the electric field components at whole time steps and the magnetic field components at half time steps. We choose the dimensions of the Yee cell to correspond to the SCFT grid of points. In this manner, the propagation of electromagnetic waves can be simulated in systems that possess nanoscale domains.

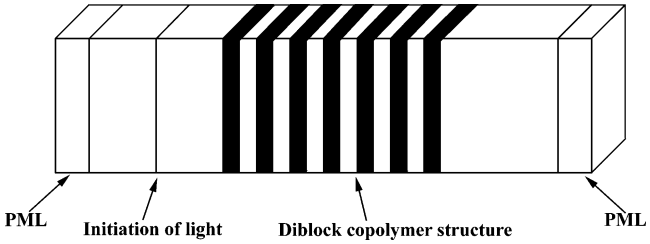

Figure 2. Structure of the FDTD simulation domain.

The above equations must be solved with the appropriate boundary conditions. To simulate free space boundary conditions, the perfectly matched layer (PML) was introduced by Berenger.[31] The PML was designed to absorb electromagnetic waves without reflection and thereby negate the system size effects that arise from the use of a finite computational domain (see Figure 2). The basic principle arises from the reflectance of a wave passing from a medium A into a medium B being given by

$$\Gamma = \frac{\eta_A - \eta_B}{\eta_A + \eta_B} \quad (7)$$

where $\eta = \sqrt{\mu/\epsilon}$ is the impedance. If ϵ changes with μ between medium A and medium B such that η remains constant, then the wave will pass through the interface between the two media without reflection. If a series of layers are matched in this manner, then a wave will pass through the layered media without impediment. However, once the wave reaches the end of this layered medium, the wave will still be reflected from the simulation boundary and propagate back into the computational domain. To simulate an absorbing boundary, the wave must be absorbed as it propagates through the PML structure. This is accomplished through the introduction of anisotropic electric and magnetic conductivities. This is equivalent to introducing complex μ and ϵ, the real part dictating the propagating part of the wave and the imaginary part dictating the attenuating component. In the PML media, the six electromagnetic fields are split into 12 different components, yielding the following Maxwell equations (for the x components):[32]

$$\epsilon \frac{\partial E_{xy}}{\partial t} + \sigma_y E_{xy} = \frac{\partial (H_{zx} + H_{zy})}{\partial y}$$

$$\epsilon \frac{\partial E_{xz}}{\partial t} + \sigma_z E_{xz} = -\frac{\partial (H_{yz} + H_{yx})}{\partial z}$$

$$\mu \frac{\partial H_{xy}}{\partial t} + \sigma_y^* H_{xy} = -\frac{\partial (E_{zx} + E_{zy})}{\partial y}$$

$$\mu \frac{\partial H_{xz}}{\partial t} + \sigma_z^* H_{xz} = \frac{\partial (E_{yz} + E_{yx})}{\partial z} \quad (8)$$

Similar expressions can be written for the y and z components.

Through the appropriate choice of parameters, the system will theoretically absorb incident waves without reflection. The conductivities must increase from zero

at the inner interface of the computational domain to a maximum value σ_{max} at the outer edge of the layer at the system boundaries. All numerical computations reported here have been performed with conductivities of the form

$$\sigma(\rho) = \sigma_{max}\left(\frac{\rho}{\delta}\right)^{\eta} \tag{9}$$

where ρ is the distance into the PML media, δ is the thickness of the PML media (corresponding to 200 cells), and η is taken as 3.5.

To carry out our studies, we first obtain the local volume fraction of the A-phase, B-phase, and particles from the SCF/DFT calculation. These local volume fractions are then used to estimate the local dielectric constants of the media in the FDTD simulation. We employ a simple rule of mixture, linearly weighting the contributions of the different components from the respective volume fractions (i.e., $\epsilon(\mathbf{r}) = \phi_A(\mathbf{r})\epsilon_A + \phi_B(\mathbf{r})\epsilon_B + \phi_P(\mathbf{r})\epsilon_P$, where ϵ_i characterizes the permittivity of the material i).[33] In the current simulations, the dielectric constants for the respective blocks are taken to be 2.53 and 2.28; these numbers fall in the range that is typical for polymeric materials.[2,34] The dielectric constant of the particles is take to be 10.2, which corresponds to the value for cadmium selenide. The spatially distributed dielectric constants are assigned to the center of mesh cells. The material properties at the nodes of a Yee cell are then averaged from the values in adjacent mesh cells.

The system exhibits a lamellar structure, which is determined through the SCF/DFT simulation. Periodic boundary conditions are applied to the system boundaries in the y and z directions (reflecting the translational invariance along y and z in the 1D SCF/DFT calculations). The periodicity of the SCF/DFT results along x (perpendicular to lamellar structure) is used to construct 48 layers of the lamellar structure in the x-direction; these layers are then sandwiched between two homogeneous regions. The size of the system, including the PML boundaries, is 3401 × 51 × 51. To minimize the reflectance of incident light from the interface between the homogeneous regions and the layered region, the homogeneous regions are assigned a dielectric constant equal to that of the pure B phase material and the layered region begins and ends in the middle of the B domain. This ensures that the reflection of light when radiated on the multilayered structure depends on the morphology of the layered structure. To establish a correlation between our simulation parameters and experimental values, and thus set up a physical length scale in our system, we equate the width of a lamellar domain obtained from the SCF/DFT for the pure symmetric diblocks to 50 nm.[2]

A differentiated Gaussian pulse, encompassing a range of frequencies, is propagated toward the periodic structure of the diblock copolymer (see Figure 2). Light of normal incidence (in the x-direction) when reflected or transmitted from the structure will always propagate in the x-direction due to the 1D nature of the structure. The fast Fourier transform (FFT) of the resultant transmitted and reflected signals then reveals the frequencies that were forbidden to propagate within the structure. The transmitted and reflected spectra can be presented relative to the FFT of the original differentiated Gaussian pulse to give the normalized transmittance and reflectance. In the current simulations, the diblock copolymer structure is assumed to be nonabsorbing, and therefore all light is either reflected by the structure or transmitted through it (i.e., reflectance + transmittance = 1).

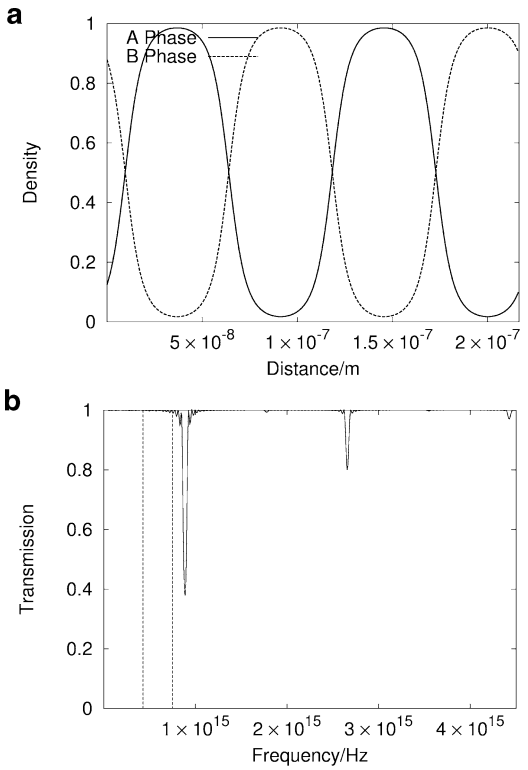

Figure 3. Symmetric unfilled diblock copolymer; $\chi_{AB}N = 20$: (a) volume fraction profiles of constituents and (b) transmittance spectra.

3. Results and Discussion

The initial case that we consider involves a symmetric diblock copolymer without the addition of the fillers. The volume fraction profiles corresponding to the A and B phases are presented with respect to distance in the x-direction in Figure 3a. As is typical in diblock copolymers, the dielectric contrast between the two phases is relatively small. If we assume that the transition between the A and B phases is instantaneous (i.e., a sharp change in the dielectric contrast between A and B), we can use a simple theory that takes into consideration the optical paths of the domains to estimate the frequencies at which reflection will occur,[35] and consequently, transmission will be reduced. The mth-order frequency is given by

$$f_m = \frac{cm}{2(d_A n_A + d_B n_B)} \tag{10}$$

where c is the speed of light, d is the width of the domain, and n is the refractive index of the domain; the subscripts A and B correspond to the A and B phases, respectively. For the above case, the principal frequency ($m = 1$) is estimated from theory to be 0.89×10^{15} Hz, which corresponds to a wavelength of 337 nm (ultraviolet).

In our calculations, we use the volume fraction profiles in Figure 3a to assign the appropriate values of the dielectric constants in the FDTD simulation; consequently, the variation in the dielectric constant

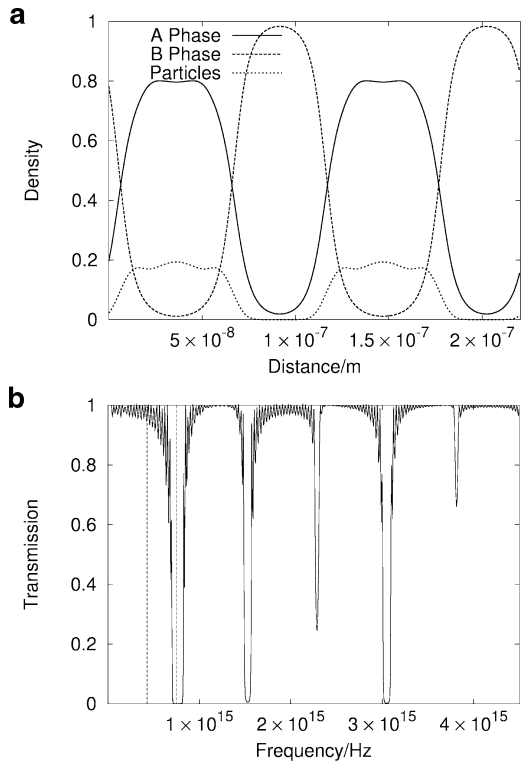

Figure 4. Symmetric filled diblock copolymer with particles localized in A phase; $\chi_{AB}N = 20$, $\chi_{AP}N = 0$, and $\chi_{BP}N = 20$: (a) volume fraction profiles of constituents and (b) transmittance spectra.

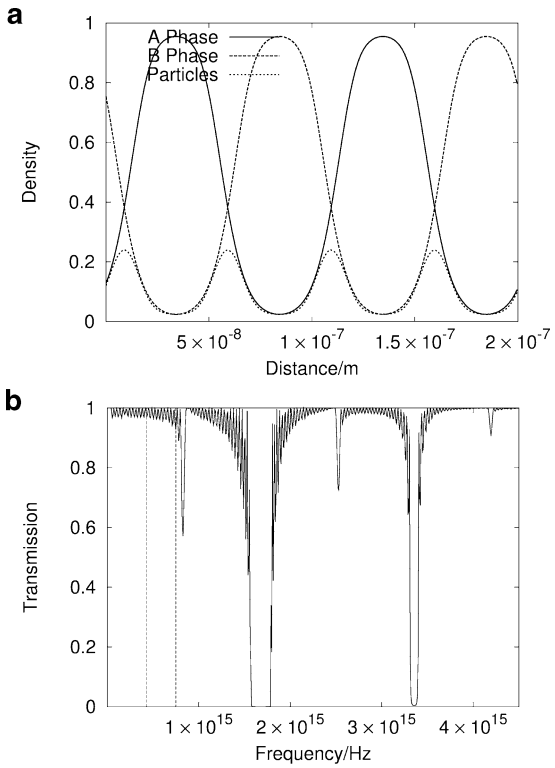

Figure 5. Symmetric filled diblock copolymer with particles localized at interface; $\chi_{AB}N = 20$, $\chi_{AP}N = 20$, and $\chi_{BP}N = 20$: (a) volume fraction profiles of constituents and (b) transmittance spectra.

between the A and B phases is relatively smooth. Nonetheless, in our studies $\chi_{AB}N = 20$, and thus, there is only a relatively small degree of overlap between these domains. Figure 3b depicts a FDTD calculation for the transmission of light as a function of the frequency of the incident light. In this plot, a value of 1 in the vertical axis corresponds to 100% transmission. We do in fact observe a decrease in transmission in the region corresponding to the principal frequency of reflection predicted from eq 10. Also of interest is the absence of even orders of reflection. The relative intensities of the various orders depend on the ratio between the optical thicknesses of the two domains (where $n_i d_i$ is the optical thickness of species i = A, B). The variable

$$g = \frac{n_A d_A}{n_A d_A + n_B d_B} \tag{11}$$

can be used to estimate these relative intensities.[35] A value of $^1/_2$ corresponds to equivalent optical distances, as is the case for a symmetric diblock with little dielectric contrast, and this results in the suppression of all even orders.[35] This can be seen in Figure 3b as the high degree of transmittance in regions that correspond to even multiples of 0.89×10^{15}.

Because of the small dielectric contrast in this system, the reflectance is small and the frequency band over which this reflectance occurs is also small. To increase the magnitude of the reflectance and the size of the band gap, the dielectric contrast between the domains must be increased. We next consider a melt of symmetric diblock copolymers that contains A-like particles. In particular, we set $\chi_{AP} = 0$ and $\chi_{BP}N = 20$. Here, and in all subsequent cases, we fix $\chi_{AB}N = 20$. In addition, the radius of the particle, R_p, is set to $0.15R_0$, where R_0 is the root-mean-squared end-to-end distance of the diblock. The total volume fraction of particles is fixed at 10% ($\phi_P = 0.1$).

As can be seen from the volume fraction profiles in Figure 4a, these fillers become localized within the A domains, which are swollen by the particles. The transmission for this system is presented in Figure 4b. This case may be distinguished from the previous unfilled case in a number of ways. First, the reflectance of light at certain frequencies is 100% (i.e., transmission is 0%), as opposed to roughly 60% in the previous system. Second, the width of the band gaps is larger, especially those corresponding to the higher orders of reflection. Third, the principal frequency of reflectance now overlaps the optical range (marked by dashed vertical lines in Figure 4b), which corresponds to light in the visible spectrum. The dielectric constant associated with the A phase is now increased due to the presence of the particles. This behavior, combined with the swelling of the A phase, gives rise to a larger optical path, $d_A n_A$. From eq 10, it can be seen that this has the effect of decreasing the frequency at which principal reflectance occurs, as is the case for the simulation results in Figure 4b.

The following and more interesting case involves a symmetric diblock copolymer melt that contains nonselective particles. Specifically, we set $\chi_{AP}N = \chi_{BP}N = 20$. Since $\chi_{AB}N$ is also equal to 20, all of the species are equally incompatible. The volume fraction profiles for this system are given in Figure 5a. As can be seen, the sizes of the A and B phases are comparable and the particles are confined at the A/B boundary. In such a mutually incompatible system ($\chi_{AP} = \chi_{BP} = \chi_{AB}$), the minority component is expelled to the interface[36] primarily because it is energetically more favorable for the A component to be surrounded by A and similarly for

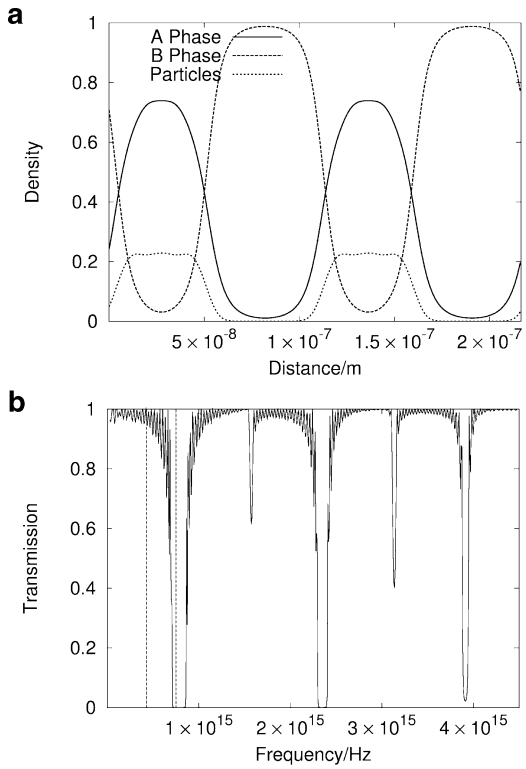

Figure 6. Asymmetric filled diblock copolymer (37:63) with particles localized in A phase; $\chi_{AB}N = 20$, $\chi_{AP}N = 0$, and $\chi_{BP}N = 20$: (a) volume fraction profiles of constituents and (b) transmittance spectra.

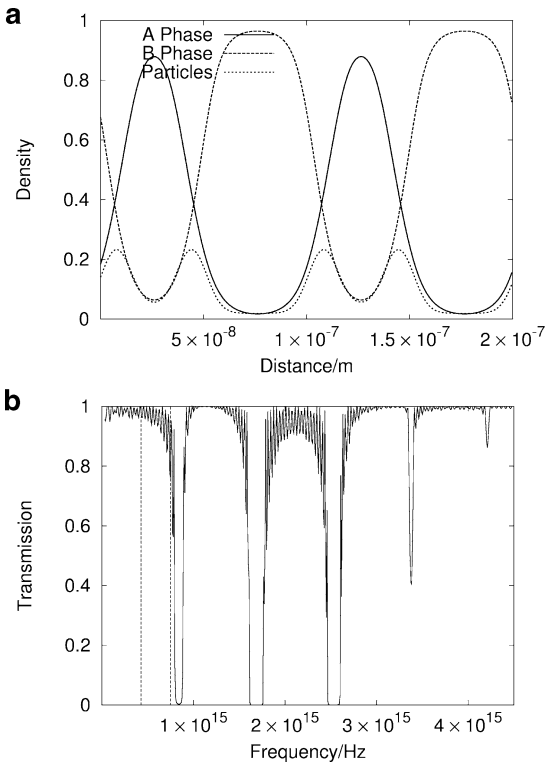

Figure 7. Asymmetric filled diblock copolymer (37:63) with particles localized at interface; $\chi_{AB}N = 20$, $\chi_{AP}N = 20$, and $\chi_{BP}N = 20$: (a) volume fraction profiles of constituents and (b) transmittance spectra.

the B component to be immersed in B. At the A/B interface, the particles increase the dielectric heterogeneity of the structure. The optical consequences of this morphology can be seen in the transmittance in Figure 5b. The gap associated with the principal frequency corresponding to the periodic structure of the diblock copolymer is narrow, and a reflectance of only 40% is observed. The more defined and much wider band gap occurs where the second order of reflection is expected to occur. This is because the relative differences between the A and B phases are small, and the principal frequency is now associated with the polymer−particle layers. The principal dielectric contrast occurs between the particles at the interface and the unfilled polymer domains. Hence, the periodicity of high dielectric contrast is now roughly half of that associated with the diblock copolymer structure. The A and B domains are slightly different, however, and small decreases in the transmittance are still observed at frequencies associated with the diblock copolymer periodicity.

We now consider the case where the diblock copolymer is no longer symmetric, but the system still displays a lamellar morphology. Figure 6a depicts the volume fraction profiles of a 37:63 diblock copolymer with the A-like particles embedded in the A phase. In this case, $\chi_{AP}N = 0$ and $\chi_{BP}N = 20$. Despite the swelling of the minority phase by the confinement of the particles, the B phase is still thicker. The transmission for this system is presented in Figure 6b. The presence of the particles increases the dielectric contrast within the system, and as in the filled systems above, wide band gaps are present with reflectances of 100%. The principal frequency of reflectance is clearly associated with the dielectric contrast between the filled A phase and the unfilled B phase. As in Figure 4b, the principal frequency band gap crosses from the violet to the ultraviolet regions of the spectrum (either side of the dashed line on the right). An interesting consequence of increasing the dielectric constant within the minority phase is that the optical path of the A phase is also increased. This results in optical paths in both phases being comparable, and similar to the unfilled symmetric system, the even orders of reflectance are suppressed.

In the final case, we investigate the inclusion of nonselective fillers at the interface of a nonsymmetric (37:63) AB diblock copolymer. Here, $\chi_{AP}N = \chi_{BP}N = 20$. The volume fraction profiles associated with this system are presented in Figure 7a. While the particles are clearly localized in the interfacial regions, there is also a small volume fraction of these fillers in the minority A domain. Since the B block is longer, the overall contact energy would be greater if the particles were to leak into the B rather than the A phase. The effect that this has on the optical properties is revealed in Figure 7b, which depicts the transmittance for this system. Because of particles in A, the dielectric contrast between the A and B phases is substantial, and therefore, the principal band gap is associated with the periodicity of the diblock copolymer and not the periodicity of the polymer−interface regions, as was the case in the equivalent symmetric system (see Figure 5). It is also worth noting that the principal band gap occurs outside the visible range of the spectrum. An interesting consequence of the clustering of particles at the interface is a decrease in the domain size. (A greater particle volume fraction at the A/B boundary results in a reduction of diblock junction points across this interface. This, in turn, results in a lower number of chains within a given domain and hence a reduction in domain size.) The decrease in domain size has the effect of increasing the principal frequency of reflection into the ultraviolet range of the spectrum.

4. Conclusions

The combination of techniques described above allowed us to determine both the morphology and optical properties of filled diblock copolymer systems. It was found that the addition of particles results in more defined band gaps, with 100% reflectance and a wider frequency gap. In addition, the increase in optical distances results in a decrease in the principal frequencies of reflectance. Furthermore, by combining the SCF/DFT and FDTD methods, we can see that changes in the chemical nature of the particles (i.e., selective vs nonselective) result in different spatial distributions of the particles and hence significantly different optical properties. In effect, this hybrid approach allows researchers to determine how choices made in the components (polymers, particles) affect the macroscopic performance of the material.

The frequencies at which light was reflected were within the violet range of the visible spectrum for certain systems containing particles. In the current simulations, the size of one lamellar domain within the pure symmetric diblock system was assumed to correspond to 50 nm. It should be noted, however, that domain sizes up to 100 nm are possible,[4] and therefore the values of the frequencies could essentially be halved. This would result in band gaps in the infrared and near-infrared ranges of the spectrum, which would be useful in the telecommunications industry.

Acknowledgment. A.C.B. gratefully acknowledges financial support from the DOE and NSF.

References and Notes

(1) Bates, F. S.; Fredrickson, G. H. *Phys. Today* **1999**, *2*, 32−38.
(2) Urbas, A. M.; Sharp, R.; Fink, Y.; Thomas, E. L.; Xenidou, M.; Fetters, L. J. *Adv. Mater.* **2000**, *12*, 812.
(3) Edrington, A. C.; Urbas, A. M.; DeRege, P.; Chen, C. X.; Swager, T. W.; Hadjichristidis, N.; Xenidou, M.; Fetters, L. J.; Joannopoulos, J. D.; Fink, Y.; Thomas, E. L. *Adv. Mater.* **2001**, *13*, 421.
(4) Fink, Y.; Urbas, A. M.; Bawendi, M. G.; Joannopoulos, J. D.; Thomas, E. L. *J. Lightwave Technol.* **1999**, *17*, 1963.
(5) Bockstaller, M.; Kolb, R.; Thomas, E. L. *Adv. Mater.* **2001**, *13*, 1783.
(6) Thompson, R. B.; Ginzburg, V. V.; Matsen, M. W.; Balazs, A. C. *Science* **2001**, *292*, 2469.
(7) Lee, J. Y.; Thompson, R. B.; Jasnow, D.; Balazs, A. C. *Phys. Rev. Lett.* **2002**, *89*, 155503.
(8) Lee, J. Y.; Thompson, R. B.; Jasnow, D.; Balazs, A. C. *Macromolecules* **2002**, *35*, 4855.
(9) Thompson, R. B.; Lee, J. Y.; Jasnow, D.; Balazs, A. C. *Phys. Rev. E* **2002**, *66*, 031801.
(10) Lee, J. Y.; Thompson, R.; Jasnow, D.; Balazs, A. C. *J. Chem. Soc., Faraday Discuss.* **2003**, *123*, 121.
(11) Thompson, R. B.; Ginzburg, V. V.; Matsen, M. W.; Balazs, A. C. *Macromolecules* **2002**, *35*, 1060.
(12) Bockstaller, M. R.; Lapetnikov, Y.; Margel, S.; Thomas, E. L. *J. Am. Chem. Soc.* **2003**, *125*, 5276.
(13) Yeh, S.-W.; Wei, K.-H.; Sun, Y.-S.; Jeng, U.-S.; Liang, K. S. *Macromolecules*, in press.
(14) Wang, Q.; Neally, P. F.; de Pablo, J. J. *J. Chem. Phys.* **2003**, *118*, 11278.
(15) Huang, C. I.; Lodge, T. P. *Macromolecules* **1998**, *31*, 3556.
(16) Fan, S.; Villeneuve, P. R.; Joannopoulos, J. D. *Phys. Rev. B* **1996**, *54*, 11245.
(17) Palkar, S. A.; et al. *Langmuir* **1998**, *14*, 3484.
(18) Krug, J. T., II; Sanchez, E. J.; Xie, X. S. *J. Chem. Phys.* **2002**, *116*, 10895.
(19) Matsen, M. W.; Bates, F. S. *Macromolecules* **1996**, *29*, 1091.
(20) There is a fundamental reason why the polymer−particle interactions should be treated differently than the particle−particle interactions. This is discussed in detail in a recent paper by Schmidt and Fuchs (ref 21). A polymer coil can effectively be thought of as a penetrable sphere of radius R_g. Hard particles whose radius is smaller than R_g can penetrate this sphere. Schmidt and Fuchs find better agreement with experimental studies on the mixing of polymers and colloids when the polymers are taken to be penetrable rather than impenetrable spheres. On the other hand, in real systems, the nanoparticles are solids and impenetrable to each other. Thus, hard-sphere interactions are needed to describe the behavior of these solid objects.
(21) Schmidt, M.; Fuchs, M. *J. Chem. Phys.* **2002**, *117*, 6308.
(22) The addition of the steric term to describe the interactions between the particles is warranted because within the free energy, not only must we capture the diblock behavior in the limit that the particle concentration approaches zero but also we must capture the behavior of the particle system as the diblock concentration approaches zero. In the limit that the particle concentration goes to zero, we are left with the SCFT expression, which has yielded good agreement with the observed experimental behavior for microphase-separated diblocks (see ref 1). In the limit that the diblock concentration goes to zero, we recover the Tarazona DFT, which again has demonstrated good agreement with experiments on the liquid/solid phase transition in particle systems (see refs 23 and 24).
(23) Tarazona, P. *Mol. Phys.* **1984**, *52*, 81.
(24) Vroege, G. J.; Lekkerkerker, H. N. W. *Rep. Prog. Phys.* **1992**, *55*, 1241.
(25) For the particle sizes that we have examined, the contribution of the "Tarazona term" or steric term to the total free energy is small; i.e., for $R = 0.15R_o$, this term is roughly 10% of the total free energy. Nonetheless, this term is important for capturing the behavior of diblock/nanoparticle systems. This is clearly illustrated in the behavior of a binary particle mixture in the diblocks (see refs 7 and 9).
(26) Matsen, M. W.; Barrett, C. *J. Chem. Phys.* **1998**, *83*, 4317.
(27) Drolet, F.; Fredrickson, G. H. *Phys. Rev. Lett.* **1999**, *109*, 4108.
(28) Bohbot-Raviv, Y.; Wang, Z.-G. *Phys. Rev. Lett.* **2000**, *85*, 3428.
(29) Maxwell, J. C. *Philos. Trans. R. Soc. London* **1865**, *155*, 459.
(30) Yee, K. S. *IEEE Trans. Antennas Prop.* **1966**, *AP-14*, 302.
(31) Berenger, J.-P. *J. Comput. Phys.* **1994**, *114*, 185.
(32) Berenger, J.-P *J. Comput. Phys.* **1996**, *127*, 363.
(33) The surface of particles will scatter electromagnetic radiation when the diameters of the particles are of the same order of magnitude as the wavelength of the light. In our simulations, we are interested in nanoparticles whose diameters are less than or comparable to 10 nm; these sizes are smaller than the wavelength in the optical regime. At much higher frequencies, the nanoparticles considered here may cause scattering, but sufficiently near the optical range of frequencies (which are of interest when considering photonic band gaps), light scattering can be assumed to be small. Thus, the use of a mixing rule, which ignores such scattering effects, is valid for the frequencies of interest in this study.
(34) *CRC Handbook of Chemisty and Physics*, 83rd ed.; CRC Publishing Co.: New York, 2003.
(35) Alfrey, T., Jr.; Gurnee, E. F.; Schrenk, W. J. *Polym. Eng. Sci.* **1969**, *9*, 400.
(36) Huang, C.; Olvera de la Cruz, M. *Phys. Rev. E* **1996**, *53*, 812.

MA034322+